Int. J. Heat Mass Transfer. Vol. 22, pp. 831–838

0017-9310/79/0601-0831 $02.00/0

THE EFFECT OF COMPOSITION ON THE BOILING RATES OF LIQUEFIED NATURAL GAS FOR CONFINED SPILLS ON WATER

JAIME A. VALENCIA-CHAVEZ* and ROBERT C. REID
LNG Research Center, Department of Chemical Engineering, Massachusetts Institute of Technology, Cambridge, MA 02139, U.S.A.

(*Received* 14 *July* 1978 *and in revised form* 20 *November* 1978)

Abstract—The rate of boiling of liquefied natural gas (LNG) spilled onto a water surface was experimentally measured in a confined area calorimeter. Increasing the concentration of ethane and propane resulted in higher boiling rates. In all cases, the vaporization rate was found to be very time dependent with concomitant variations in the LNG composition and temperature as well as in the character of the water where ice formed and increased in thickness. A qualitative theory is proposed to explain the effect of composition on the boiling rates and a quantitative model developed to predict boiling rates for LNG spills. This model is based on a numerical solution to the Stefan problem and is coupled to a vapor–liquid equilibrium model which tracks changes in LNG composition and temperature. Good agreement is obtained between predicted and experimental boiling rates with the use of a single adjustable parameter—which is itself correlated with initial LNG composition.

NOMENCLATURE

- a, Soave constant [J m^3/mol^2]; a_i, for component i;
- A, dimensionless Soave constant, equation (6);
- b, Soave constant [m^3/mol]; b_i, for component i;
- B, dimensionless Soave constant [m^3/mol];
- $\hat{f}_i$, fugacity of component i [N/m^2];
- k_I, thermal conductivity of ice [W/m^2];
- k_{ij}, interaction parameter between components i and j;
- K, dimensionless parameter defined in terms of the properties of ice and water [18];
- K_i, vaporization coefficient for component i;
- m, number of grid points chosen in the numerical solution;
- M_0, original mass spilled [g/cm^2];
- N_i, mol of i; N, total mol; N_V, mol of vapor;
- P, N_L, mol of liquid;
- q, heat flux [W/m^2];
- R, gas constant [J/mol K];
- T, temperature [K];
- T_{w0}, initial water temperature [K];
- V, volume [m^3];
- x_i, mol fraction of component i, liquid;
- y_i, mol fraction of component i, vapor;
- Z, compressibility factor, PV/NRT.

Greek symbols

- α_I, thermal diffusivity of ice [m^2/s];
- β, ratio of the density of water to that of ice;
- θ, departure temperature, $T-T_f$ [K];
- τ, time, s; τ_{cf}, time to collapse vapor film;
- ϕ_i, fugacity coefficient of component i.

Subscripts

- b, boiling temperature of LNG;
- f, freezing point of water;
- C_1, C_2, C_3, methane, ethane, propane.

THE STUDY of the transient boiling rates of cryogenic liquids spilled onto a water surface presents some novel and interesting aspects. The water can (and usually does) undergo a phase transition which modifies significantly the thermal and morphological character of the interface. The cryogenic mixture will also fractionate with concomitant variation in both composition and temperature. Liquefied natural gas (LNG) is a particularly apt cryogen to study as measured or correlated boiling rates are necessary to predict the hazards following a hypothetical accident-scenario involving an LNG tanker.

LNG is comprised primarily of methane with up to about 10% ethane and lesser quantities of nitrogen, propane, and higher aliphatic hydrocarbons. The boiling temperature at one bar is in the range of 111 K (depending upon composition) and the density is about 420–470 kg/m^3.

Most early work which considered the rate of vaporization of LNG on water [1–3] were reviewed by Drake *et al.* [4] who also reported on the boiling rates of pure liquid nitrogen, methane, ethane and a few LNG mixtures. Since the paper by Drake *et al.*, Vestal [5] studied the boiling rates of several cryogens in a Dewar flask. There is, however, a serious problem in interpretating his results since it is believed that the relatively heavy walls of the flask contributed significantly to the energy required for vaporization.

Dincer *et al.* [6], in a brief note, concluded that the initial water temperature was not an important variable in determining the boiling rates of either liquid nitrogen or liquid methane on water.

*To whom correspondence should be addressed: Arthur D. Little, Inc., 20 Acorn Park, Cambridge, MA 02140, U.S.A.

A study of the rate of vapor evolution following spills of liquefied petroleum gas (LPG) on water was described by Reid and Smith [7].

None of the LNG studies prior to the present work examined carefully the effect of LNG composition nor were definitive models developed to interpret the results in a quantitative manner.

EXPERIMENTAL

Boiling experiments were carried out in a calorimeter partially filled with distilled water. The LNG was rapidly spilled on the surface and the mass loss of the system followed as a function of time using a load cell connected to a real-time data acquisition system. The calorimeter was designed and constructed to minimize any energy transfer to the cryogen except from the water. It is shown schematically in Fig. 1. Three concentric, transparent side walls were employed. The outer was made from a 0.32 cm acrylic tube while the two inner walls were formed by bending 25 μm Mylar sheets into a cylindrical shape. 2 mm polyurethane spacers separated the tubes and dry nitrogen was used to purge the gaps prior to a test. The maximum heat transfer from the calorimeter walls was less than 1% of the energy transferred between the LNG and water.

The heat-transfer area was $\sim 140\,cm^2$. In Fig. 1, a cryogen distributor is also shown. In the spill (through the center of the distributor), vanes directed the liquid flow in a direction tangential to the surface to minimize any disturbance. As it was suspended independently of the calorimeter, any initial overshoot of the load cell was minimized.

Three vapor thermocouples were attached to the suspension rod holding the distributor. A sufficient length of thermocouple lead wire was exposed to minimize axial heat conduction through the wires.

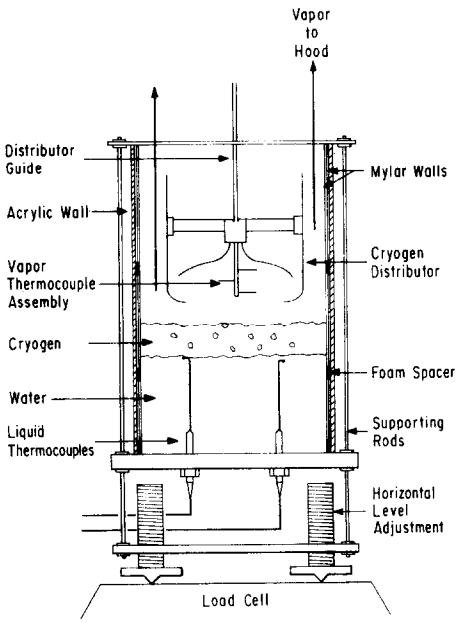

FIG. 1. Calorimeter.

The location of the thermocouple along the suspension rod could be changed. Normally, however, they were spaced 2, 3.5 and 5 cm above the maximum anticipated height of the cryogen after a spill. Six liquid thermocouples (which entered the bottom of the calorimeter) were used to follow the water and LNG temperatures.

Before any test, the composition of the LNG was determined by removing a liquid sample, evaporating it completely and employing a gas chromatograph. Special techniques had to be developed to prevent fractionation during sampling—and also to measure the nitrogen content. These are described in detail elsewhere [8].

In a few tests, vapor grab-samples were taken at various times during the experiment using fine capillary tubing connected to evacuated bulbs. The value of such data was to verify the vapor–liquid equilibrium model described next.

VAPOR–LIQUID EQUILIBRIA

LNG is comprised of components which differ significantly in volatility, viz. $N_2 > CH_4 > C_2H_6 > C_3H_8$, etc. Thus, during a transient boiling experiment, the vapor and liquid phases vary in composition (and temperature). It is tempting to assume that the liquid and vapor are always in phase equilibrium as there are then thermodynamic relationships in the literature which can be used to determine instantaneous vapor and liquid compositions (and temperatures) knowing only the initial conditions and the total mass evolved. To verify this equilibrium assumption, vapor compositions were measured as noted earlier and the results compared to those predicted from thermodynamics. Fugacity coefficients for all components were calculated by equation (1) [9].

$$\ln \phi_i = \ln(\hat{f}_i/y_i P) = \int_V^\infty \left[\left(\frac{P}{N_i} \right)_{T,V,N(j \neq i)} - \frac{RT}{V} \right] dV - \ln Z. \quad (1)$$

The P—V—T behavior of LNG was described by the Soave [10] modification of the Redlich–Kwong [11] equation of state,

$$P = \frac{NRT}{V - Nb} - \frac{N^2 a}{V(V+Nb)}. \quad (2)$$

With equation (2), equation (1) may be integrated to yield

$$\ln \phi_i = \frac{b_i}{b}(Z-1) - \ln(Z-b) + \frac{A}{B}\left[\frac{b_i}{b} - 2\sum_j \frac{(1-k_{ij})(a_i a_j)^{0.5}}{a} x_j \right] \times \ln\left(\frac{Z+B}{Z} \right), \quad (3)$$

with

$$a = \sum_j \sum_k x_j x_k (1-k_{jk})(a_j a_k)^{0.5}, \quad (4)$$

$$b = \sum_j x_j b_j, \tag{5}$$

$$A = aP/R^2T^2, \tag{6}$$

$$B = bP/RT. \tag{7}$$

The parameters a_j, b_j are found from pure component data. k_{jk} is an interaction parameter for the binary $j-k$. A detailed study of the available data for the various possible binaries in a typical LNG [12–16] yielded the values shown in Table 1. With

Table 1. Binary interaction coefficients for LNG vapor–liquid calculations

Component $i\rightarrow$ / Component $j\downarrow$	Nitrogen	Methane	Ethane	Propane
Nitrogen	—	0.035	0.035	0.120
Methane		—	0.0	0.010
Ethane			—	0.0
Propane				—

these values of k_{ij}, equation (4) was employed to calculate ϕ_i (vapor and liquid) and the distribution coefficient K_i determined.

$$K_i = \frac{y_i}{x_i} = \frac{\phi_i\,(\text{liquid})}{\phi_i\,(\text{vapor})}. \tag{8}$$

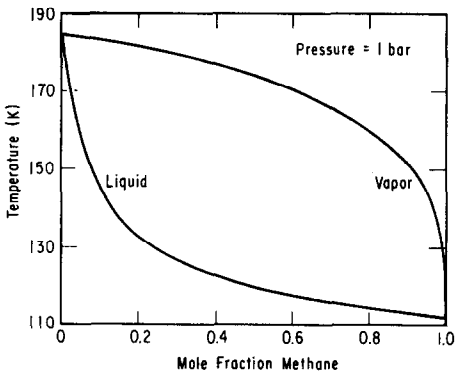

FIG. 2. Calculated temperature—composition diagram for the methane–ethane system.

Excellent agreement was attained when experimental and calculated values of K_i were compared for the available vapor–liquid equilibrium data on LNG. Temperature–composition diagrams could also be obtained; one typical result for the system methane–ethane is shown in Fig. 2. Examination of this figure reveals the important fact that for all methane concentrations exceeding about 20 mol%, the methane vapor-composition exceeds 99%. Thus, in boiling an LNG formed predominantly of methane, with some ethane (and propane), the vapor would be expected to consist essentially of pure methane until most of the methane had been volatilized.

To utilize the vapor–liquid equilibrium relations in the analysis of the boiling experiments, one can follow the change in composition by writing a differential material balance for each component $_i$,

$$-\mathrm{d}(x_i N_L) = y_i N_V. \tag{9}$$

Since $\mathrm{d}N_L = -\mathrm{d}N_V$,

$$\frac{\mathrm{d}N_L}{N_L} = \frac{\mathrm{d}x_i}{y_i - x_i}. \tag{10}$$

Equation (10) relates the change in the moles of liquid to the composition of the liquid and vapor phases. This equation can be numerically integrated using mass readings of the calorimeter as boiling proceeds. For instance, initially, N_L and x_i are known. y_i (initial) is then calculated from equation (8) and for a small ΔN_L, Δx_i can be found. The procedure is then repeated to yield values of x_i, y_i as a function of N_L.

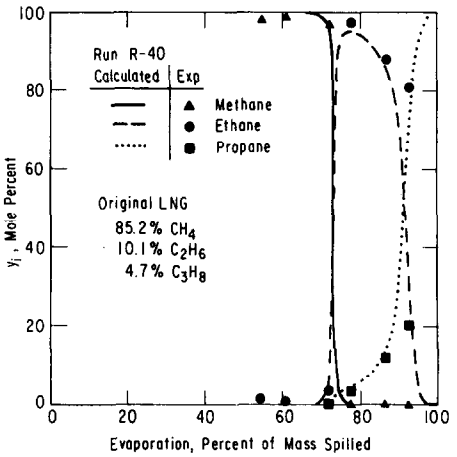

FIG. 3. Calculated and experimental vapor compositions as a function of mass evaporated.

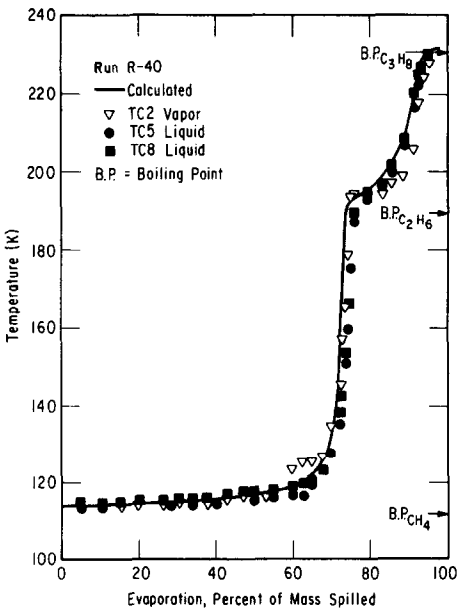

FIG. 4. Calculated and experimental temperatures as a function of mass evaporated.

To test this procedure—as well as to verify the basic assumption that vapor–liquid equilibrium exists in a transient rapid boiling of LNG—experimentally measured vapor compositions were compared with values predicted using the model outlined above. The results from one typical test are shown in Fig. 3. The model also predicts the change in LNG temperature during boiling when the more volatile components are preferentially vaporized as illustrated in Fig. 4 for the same test shown in Fig. 3.

With these encouraging results, the vapor–liquid model was incorporated into the heat-transfer analysis described below to allow one to predict the LNG temperature and composition during the boiling process.

RESULTS

Pure hydrocarbons (> 99.9%), methane, ethane, and propane were spilled on water and the mass evaporated was recorded as a function of time. Similar tests were carried out with binary mixtures of methane–ethane and ethane–propane and with ternary mixtures of methane–ethane–propane. A few tests were also made with nitrogen (< 5%) added to methane and LNG.

To allow a calculation of the *rate* of boiling, the mass boiled was correlated with time using a simple polynomial; i.e. the correlation of the mass boiled at any time τ involved fitting a polynomial through $2n+1$ points, n immediately before τ, n immediately after τ and the mass boiled off at time τ itself. The boiling rate could then be determined by evaluating the derivative of the polynomial at time τ. For the first n points (0, 1, 2, ..., n s), a polynomial was fitted through the first $2n+1$ points; the derivatives evaluated at 0, 1, 2, ..., n s were the respective boiling rates. Because the mass boiled off is not clearly defined in the first few seconds (it took a second or two to spill the cryogen), the error for these points is larger than the average error.

As an indication of the degree of error of the fit, both the root mean square deviation as well as the maximum absolute per cent error were calculated. Furthermore, the boiling rates were integrated using one of the Newton–Cotes formulas for integration, the well known Simpson's 1/3 rule.

For each point, a selection between a polynomial of first or second order was made based on the RMS error. After the first few seconds, the maximum absolute deviation in the polynomial fits were less than 1%. Upon integration of the boiling rates, the resulting mass boiled off was typically within 1 or 2% of the experimental values.

The value of n used to determine the $2n+1$ points for each polynomial was 4. However, when the boiling rates exhibited sharp peaks a value of $n = 2$ was used.

Some boiling rates for very pure liquid methane are shown in Fig. 5. A peak boiling rate is reached in about 40 s. Ice patches were noted after about 5 s and the surface was covered in about 20 s. Liquid ethane boiled more rapidly (whether expressed as g/cm^2 s or W/cm^2) than methane and a peak rate was reached in about 15 s. Ice also formed more quickly. Propane boiled very rapidly for the first few seconds then the rate decreased; ice formed almost immediately and was quite irregular (see also [7]).

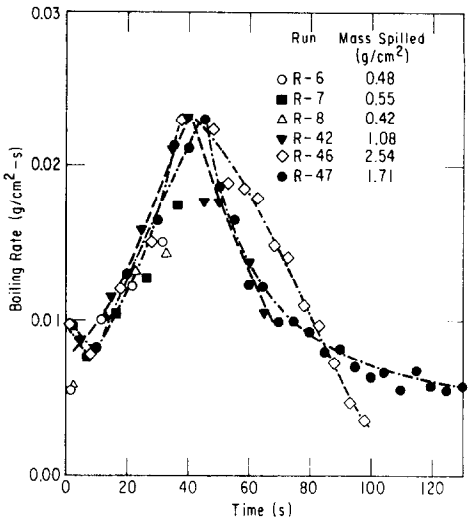

FIG. 5. Boiling rates for pure liquid methane.

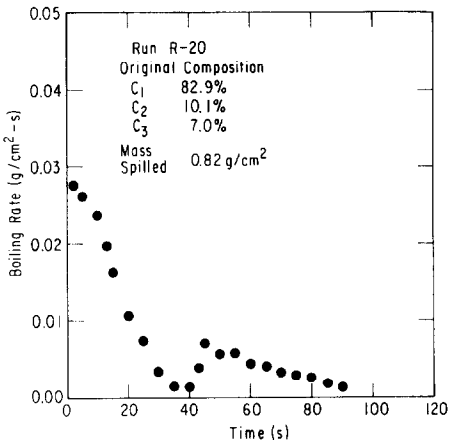

FIG. 6. Boiling rates a typical ternary LNG mixture.

Methane diluted with ethane and/or propane showed a very different boiling character than pure methane. With increased dilution, the "peak" boiling rate shifted to lower times and increased in magnitude. A typical ternary boiling-rate curve is shown in Fig. 6; in this case no "peak" is evident—at least after 1 s, the first recorded mass-datum point. Methane–ethane–propane mixtures boiled with extensive foam and ice usually appeared within a few seconds. As illustrated in Fig. 6, secondary, small peaks appeared later in the test.

Additions of a few per cent nitrogen to either methane or methane–ethane–propane mixtures did not affect the boiling rates significantly.

DISCUSSION AND ANALYSIS

Qualitative concepts

LNG consists primarily of methane (> 80–85%) and the bubble-point temperature (~ 111–120 K) is not particularly sensitive to composition. The large temperature difference between the boiling LNG and the water (~ 290–300 K) would certainly suggest that, initially, film boiling would result. Nevertheless, there are profound differences between the boiling of very pure liquid methane and LNG with even small concentrations of ethane and/or propane. The LNG boils at a higher rate, ice forms more rapidly, foam and very small vapor bubbles are observed and the "peak" boiling flux is attained in a shorter time period.

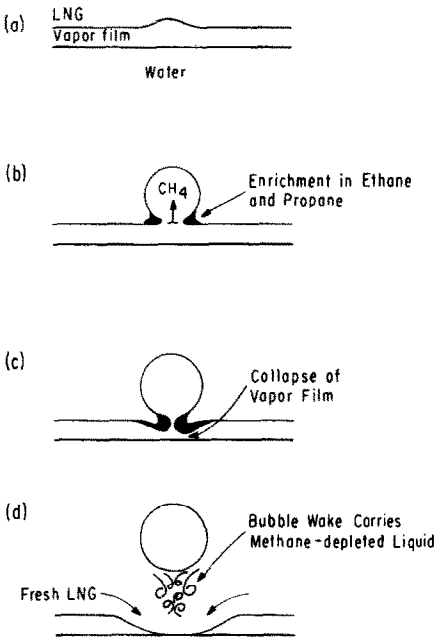

FIG. 7. Sequence of events leading to the collapse of the vapor film during boiling of LNG on water.

To explain such differences, it is suggested that LNG (and pure methane) does, in fact, film boil immediately after contacting water [see (a) in Fig. 7]. Vapor bubbles begin to form. Since there is such a large difference in the volatility of methane compared to ethane/propane, the bubbles consist almost entirely of methane. There is, therefore, an enrichment (particularly in the liquid film at the base of the bubble) in the less volatile constituents. The liquid in the proximity of the growing bubble remains essentially at the bulk liquid temperature even though a concentration gradient develops since there is a large difference between the thermal and mass diffusivities [(b), Fig. 7]. At the lower portion of the bubble, the concentrations of the ethane and propane increase with a concomitant decrease in pressure. Liquid flow occurs and the vapor film collapses near the base [(c), Fig. 7] and the buoyant bubble carries the methane-depleted liquid in its wake while fresh LNG enters and may even establish local liquid–liquid contact [(d), Fig. 7]. The cycle is then repeated. Thus the events at or near the interface increase the heat-transfer rates, small bubbles are produced and ice forms more rapidly. With ice, a surface-temperature drop occurs and eventually nucleate boiling results. With, however, a thermal resistance due to the growing ice shield, boiling rates eventually decrease.

This simple theory seems to offer a plausible mechanism to explain why there is a significant increase in the initial boiling rate of LNG as the concentration of heavy hydrocarbons is increased. These concepts are employed in the development of a quantitative heat-transfer model described below. Before this treatment, however, a few brief remarks on the shape of the later stages of the boiling curve (see Fig. 6) are necessary.

As methane is depleted in the boiling LNG, a point is reached where the boiling temperature rises quickly to a value near that for liquid ethane (see Fig. 4). This perturbation occurs when the ice–water surface is still near the methane boiling temperature. The net result is that boiling essentially ceases until the ice–water gradient has readjusted to a higher temperature level. A secondary "peak" in the heat flux then appears as ethane is vaporized. Presumably, if the LNG contained reasonable amounts of propane, this same phenomenon would be repeated as the residual LNG approached a composition rich in propane. However, for the experiments carried out in this study, when such a stage was approached, there was insufficient residual LNG to cover completely the ice–water surface.

Surface temperatures

In the complex, transient boiling process of interest in this work, it was imperative to understand how the ice–water surface temperature varied following a spill. To obtain such an estimate, it was assumed that a thin layer of ice formed almost immediately on the water surface and grew in thickness during a test. Then, employing a simple one-dimensional heat-transfer model (with a moving boundary to account for the ice growth), with experimental heat flux values, a convolution integral may be written to describe the departure of the interface temperature from its initial (assumed) value of 273 K. With θ as the surface temperature departure and τ the time after the spill,

$$\theta(\tau) = \frac{\operatorname{erf}(K\beta/2\alpha_I^{0.5})}{k_I}(\alpha_I/\pi)^{0.5} \times \int_0^{-2\sqrt{\tau}} q(\tau - u^2/4)\,du. \quad (11)$$

The thermal conductivity and thermal diffusivity of ice (k_I, α_I) are temperature averaged values. K and β are defined in the notation and q is, as noted above, the experimental heat flux.

When equation (11) was solved for a number of cases from pure hydrocarbons to rich LNG, the results indicated that θ could be correlated in a linear fashion with time. This is illustrated in Fig. 8 for two spills of methane on water at different initial temperatures. In this case, the break in the θ–τ curve was selected as the approximate time (τ_{cf}) when the film had completely collapsed. τ_{cf} values were found to be lower as the concentrations of ethane and propane were increased in the LNG spilled. An empirical correlation for τ_{cf} with composition yielded

$$\tau_{cf} = 45x_{C_1} - 40x_{C_2}^{0.2} - 10x_{C_3}^{0.1}, \qquad (12)$$

with τ_{cf} in s and x as the mole fraction. The range of equation (12) is $x_{C_2} < 0.2$, $x_{C_3} < 0.1$.

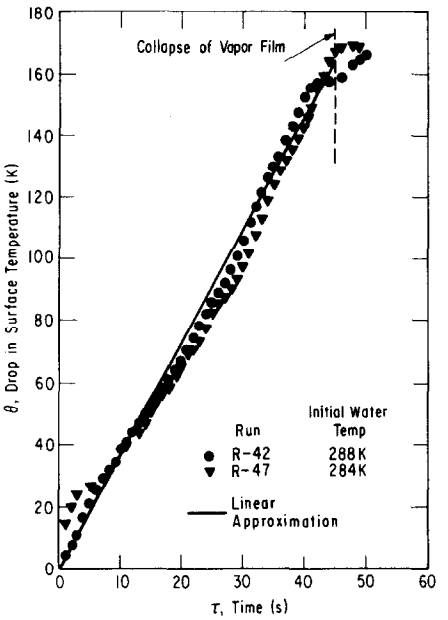

FIG. 8. Drop in surface temperature of ice after a spill of methane on water.

Variable-grid heat-transfer model

Stefan's Problem (transient heat conduction with solidification) was solved numerically allowing for a time variation in surface temperature and changes in thermal properties of the ice and water with temperature. A variable-grid size was employed with m equally sized increments dividing both the ice and water regions; the dimension of each increment was then allowed to increase as the ice layer grew. The general method is described by Murray and Landis [17] and the details of the application to the present problems are given elsewhere [8]. Two finite difference equations were obtained—one for the water and one for the ice. At the ice–water boundary, an energy balance relates the local temperature derivatives to the volumetric heat of fusion. Finally, the boundary conditions at the LNG–ice interface are

$$\begin{aligned} \theta &= (\tau/\tau_{cf})(T_b - T_f) \quad \tau < \tau_{cf}, \\ \theta &= (T_b - T_f) \qquad\quad \tau > \tau_{cf}, \end{aligned} \qquad (13)$$

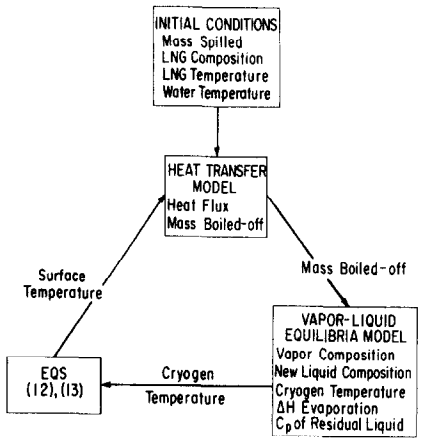

FIG. 9. Coupled heat-transfer model and vapor–liquid equilibrium model.

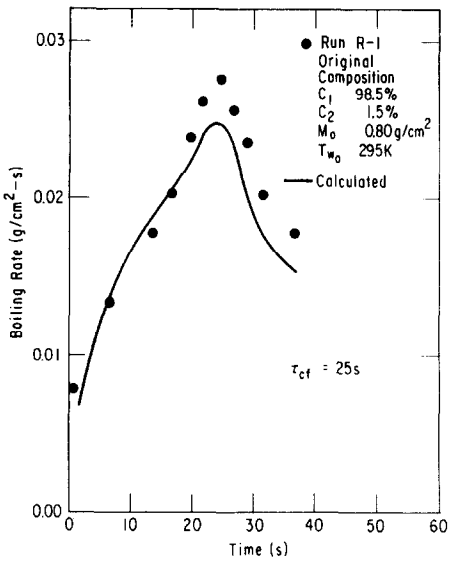

FIG. 10. Boiling rates of a methane–ethane mixture on water.

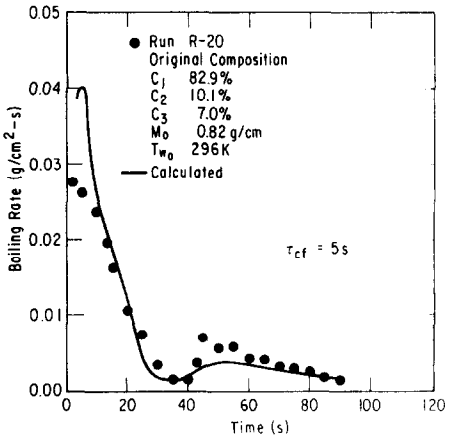

FIG. 11. Boiling rates of a methane–ethane–propane mixture on water.

where T_b is the boiling temperature of the LNG and T_f the freezing point of water. τ_{cf} was given in equation (12). Ten grid points were used ($m = 5$) and a time increment $\Delta\tau = 5$ ms was necessary to obtain stable solutions.

This numerical heat-transfer model (HTM) was coupled to the vapor–liquid model (VLE) to provide for variations in the LNG temperature as boiling occurs. The concept is illustrated in Fig. 9.

The coupled program was employed to estimate the mass–time relationships for many LNG compositions and the predicted results compared against experimental values. Typical results are shown in Figs. 10 and 11. In general the agreement between experimental and calculated was quite good considering that only one adjustable parameter was employed (τ_{cf}).

One interesting result obtained from the computer simulation was the determination of the fraction of the energy transferred from the water (ice) phase which was required to effect sensible heat changes in the LNG as the temperature rose. For rich LNG, this fraction approached unity during the rise from the methane temperature plateau to the ethane plateau—this phenomenon is, of course, reflected in the low boiling rates during this period.

In conclusion, the successful application of this heat-transfer model coupled to a vapor–liquid equilibria model suggests that the technique would also be used to simulate the transient boiling of other cryogenic mixtures on water. LPG with significant amounts of propane and butane would be an interesting system. Also, it is important to note that this study was limited to spills on a confined area surface. Experiments are now being planned to extend this study to unconfined spills of LNG on water where spreading and boiling occur simultaneously.

Acknowledgement—This research was made possible by a grant from the American Gas Association and the Gas Research Institute and their support is gratefully acknowledged.

REFERENCES

1. G. I. Boyle and A. Kneebone, Laboratory investigation into the characteristics of LNG spills on water. Evaporation, spreading, and vapor dispersion, API Report 6Z32, Shell Research Ltd., Thornton Research Centre, Chester, England (1973).
2. D. S. Burgess, J. N. Murphy and M. G. Zabetakis, Hazards associated with the spillage of LNG on water, Bureau of Mines Report RI-7448, U.S. Dept. of Interior (1970).
3. D. S. Burgess, J. Biordi and J. N. Murphy, Hazards of spillage of LNG into water, Bureau of Mines MIPR Z-70099-9-12395, U.S. Dept. Interior (1972).
4. E. M. Drake, A. A. Jeje and R. C. Reid, Transient boiling of liquefied cryogens on a water surface—I. Nitrogen, methane and ethane—II. Light hydrocarbon mixtures, *Int. J. Heat Mass Transfer* **18**, 1361–1375 (1975).
5. C. R. Vestal, Film boiling heat transfer between cryogenic liquids and water, Ph.D. Thesis, Colorado School of Mines, Golden (1973).
6. A. K. Dincer, E. M. Drake and R. C. Reid, Boiling of liquid nitrogen and methane on water. The effect of initial water temperature, *Int. J. Heat Mass Transfer* **20**, 176–177 (1977).
7. R. C. Reid and K. A. Smith, Behavior of LPG on water, *Hydrocarb. Process.* 117–121 (1978).
8. J. A. Valencia-Chavez, The effect of composition on the boiling rates of liquefied natural gas for confined spills on water, Sc.D. Thesis, Mass. Inst. of Tech., Cambridge, MA (1978).
9. J. M. Prausnitz, *Molecular Thermodynamics of Fluid-Phase Equilibria*, p. 41. Prentice-Hall, Englewood Cliffs, NJ (1969).
10. G. Soave, Equilibrium constants from a modified Redlich–Kwong equation of state, *Chem. Engng Sci.* **27**, 1197–1203 (1972).
11. O. Redlich and J. N. S. Kwong, On the thermodynamics of solutions, *Chem. Rev.* **44**, 233–244 (1949).
12. S. D. Chang and B. C. Y. Lu, Vapor–liquid equilibria in the nitrogen–methane–ethane system, *Chem. Engng Prog. Symp. Ser.* **63**, 18–27 (1967).
13. A. R. Price and R. Kobayashi, Low-temperature vapor–liquid equilibrium in light hydrocarbon mixtures: methane–ethane–propane system, *J. Chem. Engng Data* **4**, 40–52 (1959).
14. D. P. L. Poon and B. C. Y. Lu, Phase equilibria for systems containing nitrogen, methane, and propane, *Adv. Cryogen. Engng* **19**, 292–299 (1974).
15. R. Stryjek, P. S. Chappelear and R. Kobayashi, Low temperature vapor–liquid equilibria of nitrogen–methane system, *J. Chem. Engng Data* **19**, 334–339 (1974).
16. Ibid., Low temperature vapor–liquid equilibria of nitrogen–ethane system, *J. Chem. Engng Data* **19**, 340–343 (1974).
17. W. D. Murray and F. Landis, Numerical and machine solutions of transient heat-conduction problems involving melting or freezing, *J. Heat Transfer* **81**, 106–112 (1959).
18. E. R. G. Eckert and R. M. Drake, *Analysis of Heat and Mass Transfer*, p. 227. McGraw-Hill, New York (1972).

L'EFFET DE LA COMPOSITION SUR LES FLUX A L'EBULLITION DE GAZ NATURELS LIQUEFIES EN NAPPE CONFINEE SUR L'EAU

Résumé—Le flux à l'ébullition des gaz naturels liquéfiés (LNG) étendus à la surface de l'eau est mesuré dans un calorimètre confiné. L'accroissement de la concentration d'éthane et de propane provoque un acroissement des flux. Dans tous les cas, le flux de vaporisation dépend fortement du temps et des variations concomitantes de la composition des LNG et de la température aussi bien que de l'aspect de l'eau quand la glace se forme et s'épaissit. On propose une théorie qualitative pour expliquer l'effet de la composition sur le flux à l'ébullition et un modèle quantitatif prédit les flux d'ébullition pour des nappes de LNG. Ce modèle est basé sur une solution numérique du problème de Stefan et il est couplé au modèle de l'équilibre liquide–vapeur qui tient compte des changements dans la composition et la température du LNG. Un bon accord est obtenu entre les flux calculés et mesurés, avec un seul paramètre ajustable lequel est relié à la composition initiale du LNG.

DER EINFLUSS DER ZUSAMMENSETZUNG AUF DIE VERDAMPFUNGSGESCHWINDIGKEIT VON RÄUMLICH BEGRENZTEN LACHEN VERFLÜSSIGTEN ERDGASES AUF EINER WASSEROBERFLÄCHE

Zusammenfassung—Die Verdampfungsgeschwindigkeit verflüssigten Erdgases (LNG), welches auf eine Wasseroberfläche gegossen worden war, wurde mit einem Kalorimeter begrenzter Fläche gemessen. Eine Vergrößerung der Konzentration von Äthan und Propan führte zu höheren Verdampfungsgeschwindigkeiten. In allen Fällen zeigte sich eine starke Zeitabhängigkeit der Verdampfungsgeschwindigkeit mit parallel verlaufenden Änderungen in Temperatur und Zusammensetzung des LNG und zunehmender Eisbildung an der Wasseroberfläche.

Zur Erklärung des Einflusses der Zusammensetzung auf die Verdampfungsgeschwindigkeit wird eine qualitative Theorie vorgeschlagen und ein quantitatives Modell zur Berechnung der Verdampfungsgeschwindigkeit von LNG-Lachen entwickelt. Dieser Modellvorstellung liegt eine numerische Lösung des Stephan-Problems zugrunde, welche mit einem Dampf-Flüssigkeits-Gleichgewichtsmodell gekoppelt ist, in dem Änderungen der Zusammensetzung und der Temperatur des LNG berücksichtigt werden. Zwischen berechneten und gemessenen Verdampfungsgeschwindigkeiten wird durch Verwendung eines einzigen freien Koeffizienten, der seinerseits in Beziehung zur Anfangszusammensetzung des LNG steht, gute Übereinstimmung erzielt.

ВЛИЯНИЕ СОСТАВА СЖИЖЕННОГО ПРИРОДНОГО ГАЗА НА ИНТЕНСИВНОСТЬ КИПЕНИЯ НА ПОВЕРХНОСТИ ВОДЫ

Аннотация — Проведено экспериментальное измерение в калориметре интенсивности кипения сжиженного природного газа (СПГ), разлитого в виде отдельных брызг по поверхности воды. Показано, что увеличение концентрации этана и пропана приводит к увеличению интенсивности кипения. Найдено, что во всех случаях скорость испарения очень сильно зависит от времени вследствие изменений состава и температуры СПГ, а также превращения воды в лёд с возрастающей толщиной слоя. Предложена качественная теория для объяснения влияния состава на интенсивность кипения и развита количественная модель для расчёта интенсивности кипения СПГ на поверхности воды. Эта модель основана на численном решении задачи Стефана и связана с моделью равновесия системы пар-жидкость, в которой учитываются изменения в составе и температуре СПГ. С помощью обобщенного параметра, определяемого из начального состава СПГ, получено хорошее согласование между теоретическими и экспериментальными данными по интенсивности кипения.